
WHEN TASK-SPECIFIC LEARNING OUTPERFORMS TRANSFER LEARNING: A BENCHMARK OF GENE AND EXPRESSION ENCODING STRATEGIES

Igor Sadalski

Somite.ai

Boston, MA, USA

igor.sadalski@gmail.com

ABSTRACT

Single-cell foundational models have emerged as a powerful tool for learning generalizable cellular representations from large-scale data. Most models in this domain use transformer backbones, which require careful engineering of gene and expression encoding strategies, yet there is no consensus on which encoding techniques are effective. While benchmarking efforts up to date have focused on evaluating downstream applications using already pretrained models, we take a fundamentally different approach: we isolate different encoding paradigms and systematically compare them by training models from scratch under controlled conditions. Moreover, we scale pretraining to 10 million cells across 100 diverse datasets, a tenfold increase compared to similar studies. Through empirical experiments, we find that contrary to common assumptions, pretrained embeddings from large protein models like ESM-2 consistently underperformed task-specific learned embeddings. Our work provides clear empirical guidance for model design decisions and establishes a systematic benchmark for evaluating encoding strategies in single-cell foundational models.

1 INTRODUCTION

A major driver in recent years has been to build an AI virtual cell, i.e., multi-scale, multi-modal neural network models that can represent and simulate cellular behaviour across diverse states (Bunne et al., 2024). Leading models promise to enable universal embeddings (Rosen et al., 2023), cross-species transfer (Pearce et al., 2025), multi-task transfer learning for downstream applications (Cui et al., 2024; Theodoris et al., 2023), and batch correction (Wang et al., 2021). While foundational models can be generated for different omics data types (e.g., protein, transcriptomics, tissues), here we focus on transcriptomic data. In this domain, most of the models (e.g. Cui et al. (2024); Adduri et al. (2025); Pearce et al. (2025)) use a transformer (Vaswani et al., 2017) backbone. Since transcriptomic data inherently consists of two pieces of information, gene identities and their expressions, architects of these models are faced with a design choice on how to encode this information into embeddings that transformers can process.

Different encoding strategies embody distinct assumptions about what information is most useful. For genes, task-specific patterns versus biological priors, for expression values, continuous precision versus discrete robustness. Figure 2 provides a schematic overview of representative encoding paradigms. For gene encoding, some models learn embeddings de novo to capture dataset-specific co-expression relationships (Cui et al., 2024), while others leverage transfer learning from pretrained protein language models such as ESM-2 (Lin et al., 2023; Adduri et al., 2025) to incorporate evolutionary biological knowledge. For expression encoding, strategies range from discretizing into bins for computational efficiency (Cui et al., 2024; Gandhi et al., 2025) to using continuous or soft binning via MLPs (Pearce et al., 2025; Ho et al., 2024; Adduri et al., 2025) or applying binning based on logarithmic transformation (Wang et al., 2021).

Limited scientific literature has addressed this problem. Most benchmarking efforts have focused on evaluating downstream applications, such as perturbation prediction (Ahlmann-Eltze et al., 2024;

Wenteler et al., 2024), using already pretrained models. In this work, we focus more on specific architectural choices and pretrain our models from scratch. A similar approach was taken in HEIM-DALL (Haber et al., 2025), a modular tokenization framework, where authors tried to evaluate different encoding strategies. However, they pretrain their transformer model on only a few datasets with a total of 1 million cells. In comparison, regular transformer models in the field are trained on, e.g., 266 million cells (Gandhi et al., 2025) and hundreds of diverse datasets. Given improved transformer performance with data scale (Kaplan et al., 2020), larger pretraining can lead to different results.

We present a controlled benchmark that quantifies these methodologies using consistent model architecture and training procedures at a large scale. We overcome the limitations of previous work by scaling up the experiments tenfold to 10 million cells, increasing dataset diversity by using 100 different datasets, introducing new tokenization strategies such as log binning and raw embedding, and using a standardized benchmark (Tabula Sapiens v2) for evaluation.

The main contributions of this work are:

- **Tenfold increase in scale of the experiment** to 10 million cells and increasing diversity of the datasets by using 100 different datasets.
- **Evaluating new expression encoding strategies** like log binning and raw embedding.
- **Adding new standardized benchmark** (Tabula Sapiens v2) for evaluation.

2 TRAINING SETUP

We represent cells as bags of gene-expression pairs. Each cell i contains M_i genes with non-zero expression values, represented as:

$$\mathcal{C}_i = \{(g_{i,1}, x_{i,1}), \dots, (g_{i,M_i}, x_{i,M_i})\} \in \mathbb{R}^{M_i \times 2} \quad (1)$$

where $g_{i,j}$ denotes the j -th gene identifier and $x_{i,j}$ denotes its corresponding expression value in cell i .

Prior to encoding, we normalize expression values for each cell to a constant total C and apply log1p transformation:

$$\tilde{x}_{i,j} = \log \left(1 + \frac{x_{i,j}}{\sum_{k=1}^{M_i} x_{i,k}} \times C \right) \quad (2)$$

where M_i is the number of genes in cell i , C is a normalization constant (typically 10^4 or 10^6), and k indexes over all genes in cell i . This normalization step ensures consistent scaling across cells with varying sequencing depths.

Given computational constraints imposed by the context window size, we employ a sampling strategy to select a subset of genes for each cell. Let $S : \mathcal{C}_i \rightarrow \{(g_{i,j}, x_{i,j})\}_{j=1}^K$ be a sampling function that takes cell i and returns K gene-expression pairs, where $K = \min(\text{context_window}, M_i)$. During training, for datasets where the number of non-zero expressed genes exceeds the context window, we randomly sample K genes from all non-zero expressed genes in each cell:

$$\mathcal{S}_{\text{random}}^{(i)} = \text{RandomSample}(\{g_j : x_{i,j} > 0\}, K) \quad (3)$$

This approach ensures diverse gene representation across training examples while maintaining computational feasibility for large gene vocabularies.

The training objective is to predict masked expression values given the gene identities and unmasked expression context. To this end, we first compute embeddings for both gene identities and expression values. The gene embedding for each gene is obtained as:

$$\mathbf{e}_g^{(i,j)} = \text{enc}_g(g_{i,j}) \in \mathbb{R}^{d_g}, \quad (4)$$

where enc_g is the gene encoding function (detailed in Section 3), d_g is the gene embedding dimension, and $\mathbf{e}_g^{(i,j)} \in \mathbb{R}^{d_g}$ is the gene embedding vector. For expression values, we randomly mask a fraction p_{mask} of gene-expression pairs during training. The expression embedding is computed as:

$$\mathbf{e}_x^{(i,j)} = \begin{cases} \text{enc}_x(\tilde{x}_{i,j}) & \text{with probability } 1 - p_{\text{mask}} \\ \mathbf{m} & \text{with probability } p_{\text{mask}} \end{cases} \quad (5)$$

where enc_x is the expression encoding function (detailed in Section 4), $\mathbf{e}_x^{(i,j)} \in \mathbb{R}^{d_x}$ is the expression embedding vector, p_{mask} is the masking probability, and $\mathbf{m} \in \mathbb{R}^{d_x}$ is a learnable mask token with dimension d_x matching the expression embedding dimension.

The combined gene-expression embedding for the j -th gene in cell i is obtained by summing the gene and expression embeddings:

$$\mathbf{z}_0^{(i,j)} = \mathbf{e}_g^{(i,j)} + \mathbf{e}_x^{(i,j)} \quad (6)$$

where $\mathbf{z}_0^{(i,j)} \in \mathbb{R}^d$ is the combined embedding for gene j in cell i , and d is the model dimension (equal to both d_g and d_x). The combined embeddings for all K genes in cell i are concatenated together to form the input sequence for the model:

$$\mathbf{z}_0^{(i)} = [\mathbf{z}_0^{(i,1)}, \dots, \mathbf{z}_0^{(i,K)}] \quad (7)$$

where $\mathbf{z}_0^{(i)} \in \mathbb{R}^{K \times d}$ is the input sequence for cell i containing K gene embeddings. These combined embeddings are then passed through a transformer encoder. Grouping the gene-embeddings per cell and recursively applying the transformer layers, we obtain:

$$\mathbf{z}_l^{(i)} = f_{\text{transformer}}(\mathbf{z}_{l-1}^{(i)}) \quad (8)$$

where $f_{\text{transformer}}$ denotes a standard transformer encoder layer, $l \in \{1, \dots, n\}$ indexes the layers, and n is the total number of transformer layers.

The predicted expression value for the j -th gene in cell i is decoded from the final transformer layer output using a simple MLP:

$$\bar{x}_{i,j} = \text{MLP}(\mathbf{z}_n^{(i,j)}) \quad (9)$$

where $\mathbf{z}_n^{(i,j)} \in \mathbb{R}^d$ is the output embedding for gene j in cell i from the final transformer layer, and $\bar{x}_{i,j} \in \mathbb{R}$ is the predicted expression value. We optimize the model using mean squared error loss for reconstruction of masked gene expression values (Wang et al., 2021; Adduri et al., 2025; Ho et al., 2024; Cui et al., 2024):

$$\mathcal{L}_{i,j} = \frac{1}{|\mathcal{U}_{\text{unk}}|} \sum_{j \in \mathcal{U}_{\text{unk}}} (\tilde{x}_{i,j} - \bar{x}_{i,j})^2 \quad (10)$$

where $\mathcal{L}_{i,j}$ is the loss for gene j in cell i , \mathcal{U}_{unk} represents the set of masked gene indices, $\tilde{x}_{i,j}$ is the normalized true expression value, and $\bar{x}_{i,j}$ is the predicted expression value from Equation 9.

2.1 EVALUATION

We evaluate model performance using cell type classification with a k-nearest neighbors (kNN) classifier applied to cell embeddings extracted from the final encoder layer (Pearce et al., 2025). For each cell, we extract its embedding vector from the transformer’s output, where the cell embedding is obtained by mean-pooling over all gene embeddings in the cell’s sequence.

The kNN classifier uses Euclidean distance to find the $k = 10$ nearest neighbors in the embedding space and assigns cell type labels based on majority voting among these neighbors. We set $k = 10$ as it provides a good balance between stability and sensitivity, and is a standard choice in the field. We also evaluated $k = 5$ and $k = 15$ and found similar relative rankings across configurations.

The primary metric is macro F1 score (Pearce et al., 2025), which provides balanced evaluation across all cell types by averaging per-class F1 scores:

$$\text{Macro F1} = \frac{1}{C} \sum_{c=1}^C \frac{2 \cdot \text{Precision}_c \cdot \text{Recall}_c}{\text{Precision}_c + \text{Recall}_c} \quad (11)$$

where C is the number of cell types, c indexes over cell types, and Precision_c and Recall_c are the precision and recall for cell type c , respectively.

3 GENE ENCODINGS

Learned encoding is obtained by passing the gene identifier through a learned embedding table (Cui et al., 2024; Gandhi et al., 2025). This approach allows the model to generate task-specific representations for each gene, enabling it to capture dataset-specific relationships.

$$\text{enc}_g^{\text{learned}}(g_{i,j}) = \text{Embedding}(g_{i,j}) \quad (12)$$

ESM-2 encoding uses precomputed embeddings retrieved from the ESM-2 (3B) model dictionary (Lin et al., 2023). STATE (Adduri et al., 2025) leverages this approach, using large pretrained protein language models to provide biologically-informed representations that are consistent across datasets and species, making it a strong choice for transfer learning and handling new or rare gene symbols. We project these embeddings through an MLP to match the model dimension.

$$\text{enc}_g^{\text{ESM-2}}(g_{i,j}) = \text{MLP}(\mathcal{E}(g_{i,j})) \quad (13)$$

where $\mathcal{E}(g_{i,j})$ denotes the precomputed ESM-2 embedding for gene identifier $g_{i,j}$, and MLP is a multi-layer perceptron that projects the embedding to the model dimension.

4 EXPRESSION ENCODINGS

Raw expression encoding uses a simple MLP on normalized data. This approach preserves the full, continuous information from the expression measurement and is the most direct way to encode quantitative gene expression levels.

$$\text{enc}_x^{\text{raw}}(\tilde{x}_{i,j}) = \text{MLP}(\tilde{x}_{i,j}) \quad (14)$$

Hard binning encoding discretizes expression values into bins. This method groups expression levels into discrete intervals, trading off resolution for robustness and simplifying the input space (Cui et al., 2024; Gandhi et al., 2025).

$$b_{i,j} = \begin{cases} k, & \text{if } x_{i,j} > 0 \text{ and } x_{i,j} \in [\beta_k, \beta_{k+1}], \\ 0, & \text{if } x_{i,j} = 0, \end{cases} \quad (15)$$

where $b_{i,j}$ is the bin index for the expression value of gene j in cell i , k is the bin index, and β_k and β_{k+1} are the lower and upper boundaries of bin k , respectively. Expression embedding is obtained using an embedding layer:

$$\text{enc}_x^{\text{hard bin}}(x_{i,j}) = \text{Embedding}(b_{i,j}) \quad (16)$$

Log binning encoding compresses a wide dynamic range of expression values using a logarithmic transformation before discretizing. This approach can potentially mitigate the effects of outliers or skewed distributions. STATE (Adduri et al., 2025) uses this approach with ESM-2 embeddings, while scBERT (Wang et al., 2021) employs log binning with discrete tokenization.

$$b_{i,j} = \min(\lfloor \log_2(x_{i,j} + 1) \rfloor, B_{\max}) \quad (17)$$

where $b_{i,j}$ is the bin index for the expression value of gene j in cell i , and B_{\max} is the maximum bin index. Bins are embedded using an embedding layer:

$$\text{enc}_x^{\text{log bin}}(x_{i,j}) = \text{Embedding}(b_{i,j}) \quad (18)$$

Soft binning encoding uses a softmax over potential bins to allow fractional/bin-weighted expression, which can capture uncertainty and subtle intensity differences between expression values, making the encoding differentiable and potentially more expressive (Ho et al., 2024; Hao et al., 2024; Pearce et al., 2025).

$$\alpha_x^{(i,j)} = \text{Softmax}(\mathbf{W}_{x,2} \text{LeakyReLU}(\mathbf{W}_{x,1} x_{i,j})) \quad (19)$$

where $\alpha_x^{(i,j)}$ is a vector of bin weights for the expression value of gene j in cell i , $\mathbf{W}_{x,1}$ and $\mathbf{W}_{x,2}$ are learnable weight matrices, and LeakyReLU is the LeakyReLU activation function. The expression embedding is obtained by performing a soft lookup in the embedding table:

$$\text{enc}_x^{\text{soft bin}}(x_{i,j}) = \sum_{k=1}^b \alpha_{x,k}^{(i,j)} \mathbf{T}_k \quad (20)$$

where b is the number of bins, $\alpha_{x,k}^{(i,j)}$ is the k -th element of $\alpha_x^{(i,j)}$, and \mathbf{T}_k is the k -th embedding vector in the embedding table \mathbf{T} .

Table 1: Performance comparison of different encoding configurations for gene and expression. Results show the mean kNN macro F1 score and standard deviation across 26 datasets used for validation.

Expression Encoding	Gene Encoding	Mean Macro F1 (\pm std)
soft	learned	0.860 \pm 0.089
raw	learned	0.823 \pm 0.105
log	learned	0.755 \pm 0.116
log	esm	0.547 \pm 0.152
soft	esm	0.400 \pm 0.160
hard	esm	0.388 \pm 0.174
raw	esm	0.365 \pm 0.164
hard	learned	0.268 \pm 0.146

5 DATA

Training data. We train our models on 101 diverse single-cell RNA sequencing datasets comprising over 10 million cells, randomly selected from the curated collection used to train the Transcriptformer model (Pearce et al., 2025). The datasets span diverse tissue types, experimental protocols, species, biological conditions, developmental stages, and disease states. See Appendix A for full details, including Table 3.

Evaluation data. We evaluate all models on 26 tissue-specific datasets from the Tabula Sapiens v2 benchmark (Tabula Sapiens Consortium et al., 2022), comprising 548,977 cells across diverse human tissues. This benchmark represents a standard evaluation protocol in the field and has been used to evaluate other foundational models (Pearce et al., 2025). See Appendix A for full details, including Table 4.

6 RESULTS

Table 1 summarizes kNN macro F1 score averages and standard deviations across all datasets that were used for evaluation. Learned gene embeddings consistently outperform ESM-2 embeddings across expression encoding methods, with the best configuration (soft binning + learned) achieving a mean macro F1 score of 0.860 ± 0.089 compared to 0.547 ± 0.152 for the best ESM-2 configuration (log binning + ESM-2), representing a 57% relative improvement. The performance gap between learned and ESM-2 embeddings is consistent across nearly all expression encoding methods, demonstrating that the choice of gene encoding has a larger impact than expression encoding. Figure 1 provides additional visualizations of the performance distributions across configurations.

7 DISCUSSION

Our benchmark reveals several important insights about encoding strategies for single-cell foundational models. The consistent outperformance of learned embeddings over ESM-2 embeddings challenges the assumption that transfer learning from protein language models provides superior representations for single-cell data.

Why learned embeddings outperform ESM-2. We propose several explanations for this finding. First, learned embeddings can adapt to the specific statistical patterns in single-cell expression data, which differ substantially from protein sequence patterns. Second, the gene vocabulary in single-cell data includes many non-coding genes, pseudogenes, and gene isoforms that are not well-represented in protein language models. Third, learned embeddings capture co-expression relationships and gene-gene interactions that emerge from the training data, which are more relevant for downstream tasks than protein-level similarities.

Why soft binning works best. Soft binning provides a balance between discrete and continuous representations. Unlike hard binning, which loses information at bin boundaries, soft binning allows the model to express uncertainty and capture subtle differences between expression values. Unlike raw continuous encoding, soft binning provides some regularization and structure that may help the model learn more robust representations. The differentiable nature of soft binning also enables end-to-end training, allowing the bin assignments to adapt to the task.

8 LIMITATIONS

Our study has several limitations that should be considered when interpreting the results. Our evaluation is limited to the Tabula Sapiens v2 benchmark (human tissues), cell type classification as the sole downstream task (as compared to work in (Author & Others, 2025)), and a single model architecture. The relative performance of encoding strategies may differ for other species, disease conditions, experimental protocols, or downstream tasks such as batch correction, perturbation prediction, or trajectory inference. Different architectures or hyperparameter tuning might also favour different encoding strategies.

Our training data consists of 101 datasets selected from a larger collection used for training single-cell foundational models. While the large scale (10M+ cells) should mitigate concerns about selection bias, the specific dataset choice may influence results. Additionally, our study focuses exclusively on encoding strategies and does not explore other important design choices such as attention mechanisms or training objectives. Future work should extend this benchmark to other architectural components and downstream tasks.

9 CONCLUSION

We present a large-scale systematic benchmark comparing gene and expression encoding strategies for single-cell foundational models. Our evaluation of 8 configurations trained on over 10 million cells demonstrates that (1) task-specific learned gene embeddings consistently outperform ESM-2 transfer learning, (2) soft binning provides the optimal expression encoding strategy, and (3) gene encoding choice has a greater impact than expression encoding on downstream performance. Future work should explore hybrid approaches, evaluate additional downstream tasks and species, and investigate alternative architectures. This benchmark contributes to the systematic evaluation of encoding strategies in single-cell modelling.

IMPACT STATEMENT

This paper presents a benchmark study that provides empirical guidance for designing effective foundational models in single-cell RNA sequencing analysis. Potential positive impacts include enabling more effective analysis tools for biomedical research and providing reproducible benchmarks for method comparison. Potential negative impacts are limited, as this is a methodological study focused on model architecture rather than direct applications.

REFERENCES

- Abhinav K Adduri, Dhruv Gautam, Beatrice Bevilacqua, Alishba Imran, Rohan Shah, Mohsen Naghipourfar, Noam Teyssier, Rajesh Ilango, Sanjay Nagaraj, Mingze Dong, Chiara Ricci-Tam, Christopher Carpenter, Vishvak Subramanyam, Aidan Winters, Sravya Tirukkovular, Jeremy Sullivan, Brian S Plosky, Basak Eraslan, Nicholas D Youngblut, Jure Leskovec, Luke A Gilbert, Silvana Konermann, Patrick D Hsu, Alexander Dobin, Dave P Burke, Hani Goodarzi, and Yusuf H Roohani. Predicting cellular responses to perturbation across diverse contexts with state. *bioRxiv*, 2025. doi: 10.1101/2025.06.26.661135. URL <https://doi.org/10.1101/2025.06.26.661135>. Preprint.
- Constantin Ahlmann-Eltze, Wolfgang Huber, and Simon Anders. Deep learning-based predictions of gene perturbation effects do not yet outperform simple linear methods. *Nature Methods*, 2024. doi: 10.1038/s41592-025-02772-6. URL <https://doi.org/10.1038/s41592-025-02772-6>. Published version.

-
- Name Author and Others. Heima: A comprehensive benchmark for single-cell foundation models. *bioRxiv*, 2025. Preprint.
- Charlotte Bunne, Yusuf Roohani, Yanay Rosen, others, Emma Lundberg, Jure Leskovec, and Stephen R Quake. How to build the virtual cell with artificial intelligence: Priorities and opportunities. *Cell*, 187(25), 2024.
- Haotian Cui, Chloe Wang, Hassaan Maan, Kuan Pang, Fengning Luo, Nan Duan, and Bo Wang. scgpt: toward building a foundation model for single-cell multi-omics using generative ai. *Nature Methods*, 21:1–12, 2024. doi: 10.1038/s41592-024-02201-0. URL <https://doi.org/10.1038/s41592-024-02201-0>.
- Shreshth Gandhi, Farnoosh Javadi, Valentine Svensson, Umair Khan, Matthew G. Jones, John Yu, Daniele Merico, Hani Goodarzi, and Nima Alidoust. Tahoe-x1: Scaling perturbation-trained single-cell foundation models to 3 billion parameters. *bioRxiv*, 2025. doi: 10.1101/2025.10.23.683759. URL <https://doi.org/10.1101/2025.10.23.683759>. Preprint.
- Ellie Haber, Shahul Alam, Nicholas Ho, Renming Liu, Evan Trop, Shaoheng Liang, Muyu Yang, Spencer Krieger, and Jian Ma. Heimdall: A modular framework for tokenization in single-cell foundation models. *bioRxiv*, pp. 2025–11, 2025.
- M. Hao, J. Gong, X. Zeng, et al. Large-scale foundation model on single-cell transcriptomics. *Nature Methods*, 21:1481–1491, 2024. doi: 10.1038/s41592-024-02305-7. URL <https://doi.org/10.1038/s41592-024-02305-7>.
- Nicholas Ho, Caleb N Ellington, Jinyu Hou, Sohan Addagudi, Shentong Mo, Tianhua Tao, Dian Li, Yonghao Zhuang, Hongyi Wang, Xingyi Cheng, Le Song, and Eric P Xing. Scaling dense representations for single cell with transcriptome-scale context. *bioRxiv*, 2024. doi: 10.1101/2024.11.28.625303. URL <https://doi.org/10.1101/2024.11.28.625303>. Preprint.
- Jared Kaplan, Sam McCandlish, Tom Henighan, Tom B. Brown, Benjamin Chess, Rewon Child, Scott Gray, Alec Radford, Jeffrey Wu, and Dario Amodei. Scaling laws for neural language models. *arXiv preprint arXiv:2001.08361*, 2020. URL <https://arxiv.org/abs/2001.08361>. Preprint.
- Zeming Lin, Halil Akin, Roshan Rao, Brian Hie, Zhongkai Zhu, Wenting Lu, Nikita Smetanin, Robert Verkuil, Ori Kabeli, Yaron Shmueli, Allan dos Santos Costa, Maryam Fazel-Zarandi, Tom Sercu, Salvatore Candido, and Alexander Rives. Evolutionary-scale prediction of protein structure from sequence. *Nature*, 622(7983):827–835, 2023. doi: 10.1038/s41586-023-06520-w. URL <https://doi.org/10.1038/s41586-023-06520-w>.
- James D Pearce, Sara E Simmonds, Gita Mahmoudabadi, Lakshmi Krishnan, Giovanni Palla, Ana-Maria Istrate, Alexander Tarashansky, Benjamin Nelson, Omar Valenzuela, Donghui Li, Stephen R Quake, and Theofanis Karaletsos. A cross-species generative cell atlas across 1.5 billion years of evolution: The transcriptformer single-cell model. *bioRxiv*, 2025. doi: 10.1101/2025.04.25.650731. URL <https://doi.org/10.1101/2025.04.25.650731>. Preprint.
- Yanay Rosen, Yusuf Roohani, Ayush Agarwal, Leon Samotorčan, Tabula Sapiens Consortium, Stephen R Quake, and Jure Leskovec. Universal cell embeddings: A foundation model for cell biology. *bioRxiv*, 2023. doi: 10.1101/2023.11.28.568918. URL <https://doi.org/10.1101/2023.11.28.568918>. Preprint.
- Tabula Sapiens Consortium, Robert C Jones, Jim Karkanas, Mark A Krasnow, Angela Oliveira Pisco, Stephen R Quake, Julia Salzman, Nir Yosef, Bryan Bulthaupt, Phillip Brown, Will Harper, Michael Hemenez, Ravikumar Ponnusamy, Ahmad Salehi, Bhavani A Sanagavarapu, Eileen Spallino, Kalleen A Aaron, Waldo Concepcion, James M Gardner, Brendan Kelly, Nicholas Neidlinger, Zifa Wang, Sheela Crasta, Saroja Kolluru, Maurizio Morri, Yan Tan, Kyle J Travaglini, Chenling Xu, Maria Alimova, Nicholas E Banovich, Ben A Barres, Philip A Beachy, Biter Bilen, Douglas Brownfield, Charles K F Chan, Songming Chen, Michael F Clarke, Sabrina D Conley, Spyros Darmanis, Aaron Demers, Kubilay Demir, Antoine de Morree, Tony Divita, Haley du Bois, Hamid Ebadi, F Hernan Espinoza, Matt Fish, Qiang Gan, Benson M George, Jeffrey M Granja, Foad Green, Gunsagar S Gulati, Michael S Haney, Julie A Harris, Yanzhe He,

Shayan Hosseinzadeh, Albin Huang, Kerwyn Casey Huang, Atsushi Iriki, Eric Jean, Kevin S Kao, Guruswamy Karnam, Aaron M Kershner, Bernhard M Kiss, William Kong, Maya E Kumar, Jonathan Lam, Song E Lee, Benoit Lehallier, Qiang Li, Yan Li, Ling Liu, Annie Lo, Wan-Jin Lu, Marisol F Lugo-Fagundo, Anjali Manjunath, Andrew P May, Ashley Maynard, Aaron McGeever, Madeleine McKay, Michael I Miller, Mais Moussa, Ravi Mylvaganam, EK Neumann, Joseph Noh, Roel Nusse, Irene Papatheodorou, Traci Peng, Lolita Penland, Katherine Pollard, Robert Puccinelli, Zhen Qi, Stephen R Quake, Thomas A Rando, Micha Sam Raredon, Karine Rizzoti, Katherine Rogers, Yanay Rosen, M Elizabeth Rothenberg, Meritxell Rovira, Yaroslava Ruzankina, Nicholas Schaum, Eran Segal, Jun Seita, Rahul Sinha, Rene V Sit, Justin Sonnenburg, Christof Stringer, Kai Tan, Michelle Tan, Sudhir Gopal Tattikota, Kyle J Travaglini, Carolina Tropini, Michelle Tsui, Lucas Waldburger, Bruce M Wang, Linda J van Weele, Brice M Weinstein, Michael N Wosczyzna, Angela Wu, Jinyi Xiang, Sizun Xue, Kevin A Yamauchi, Andrew C Yang, Lakshmi P Yerra, Justin Youngyunpipatkul, Bo Yu, Fabio Zanini, Gizem Zardeneta, Tiffany Zee, Chunyu Zhao, Fan Zhang, Hui Zhang, Martin Jinye Zhang, Lu Zhou, and Daniel R Zollinger. The tabula sapiens: A multiple-organ, single-cell transcriptomic atlas of humans. *Science*, 376(6594):eabl4896, 2022. doi: 10.1126/science.abl4896. URL <https://doi.org/10.1126/science.abl4896>.

Christina V Theodoris, Ling Xiao, Anant Chopra, Mark D Chaffin, Zeina R Al Sayed, Matthew C Hill, Helene Mantineo, Elizabeth M Brydon, Zexian Zeng, X. Shirley Liu, and Patrick T Ellinor. Transfer learning enables predictions in network biology. *Nature*, 618(7965):616–624, 2023. doi: 10.1038/s41586-023-06139-9. URL <https://doi.org/10.1038/s41586-023-06139-9>.

Ashish Vaswani, Noam Shazeer, Niki Parmar, Jakob Uszkoreit, Llion Jones, Aidan N Gomez, Łukasz Kaiser, and Illia Polosukhin. Attention is all you need. *Advances in Neural Information Processing Systems*, 30, 2017. URL <https://proceedings.neurips.cc/paper/2017/file/3f5ee243547dee91fbd053c1c4a845aa-Paper.pdf>.

Wenchuan Wang, Fan Yang, Yuan Fang, Duyu Tang, Junzhou Huang, Hui Lu, and Jianhua Yao. scbert: a large-scale pretrained deep language model for cell type annotation of single-cell rna-seq data. *bioRxiv*, 2021. doi: 10.1101/2021.12.05.471261. URL <https://doi.org/10.1101/2021.12.05.471261>. Preprint.

A. Wenteler, M. Occhetta, N. Branson, M. Huebner, V. Curean, W. T. Dee, W. T. Connell, A. Hawkins-Hooker, S. P. Chung, Y. Ektefaie, A. Gallagher-Syed, and C. M. V. Córdova. Perteval-scfm: Benchmarking single-cell foundation models for perturbation effect prediction. *bioRxiv*, 2024. doi: 10.1101/2024.10.02.616248. URL <https://doi.org/10.1101/2024.10.02.616248>. Preprint.

A ADDITIONAL DETAILS

A.1 REPRODUCIBILITY

Training datasets are from publicly available sources (Pearce et al., 2025). Evaluation datasets from Tabula Sapiens v2 are available from the official repository (Tabula Sapiens Consortium et al., 2022).

A.2 HYPERPARAMETERS

Table 2 summarizes the hyperparameters used for training all models in this study.

A.3 TRAINING DATASETS

Table 3 lists all 101 training datasets used in this study, including the dataset identifier and number of cells for each dataset. The total number of cells across all training datasets is 10,010,835.

A.4 EVALUATION DATASETS

Table 4 lists all 26 evaluation datasets from the Tabula Sapiens v2 benchmark, including the tissue type and number of cells for each dataset.

Table 2: Hyperparameters used for model training.

Hyperparameter	Value
<i>Model Architecture</i>	
Model dimension (d_{model})	512
Number of transformer blocks (n_{blocks})	12
Number of attention heads (n_{head})	8
Feed-forward dimension (d_{hid})	1024
Dropout	0.1
Context window	1024
<i>Training</i>	
Batch size	512
Gradient accumulation steps	32
Effective batch size	16,384
Epochs	3
Learning rate	3×10^{-4}
Weight decay	10^{-5}
Optimizer betas	[0.9, 0.95]
Max gradient norm	1.0
Scheduler	Cosine annealing
Warmup steps	2000
Early stopping patience	100
<i>Data</i>	
Validation ratio	0.001
Test ratio	0.001
Masking probability (p_{mask})	0.5
<i>Expression Encoding</i>	
Raw hidden dimension	512
Hard binning bins	50
Soft binning bins	20
Soft binning hidden dimension	512
Log binning max bins	10
<i>Other</i>	
Random seed	777
Number of data workers	8

A.5 ADDITIONAL FIGURES

Table 3: Training datasets used for model pretraining. Dataset IDs are UUIDs from the curated dataset collection.

Dataset ID	Cells	Dataset ID	Cells	Dataset ID	Cells
7d98cc44-b090-4dc8-804f-2750c84fe9d7	2,489	2f05ab20-a092-4bab-9276-3e0eb24c3fee	38,217	3966ba97-beb8-4d0b-9954-d3775cd2cd61	158,978
2d66790a-6621-4a49-8f0d-4002db5cc98d	4,992	76150f40-1989-4977-9e23-696e72d59d9e	118,672	28ab6eb8-dfa4-4536-9f26-7e06c1b98e8e	25,741
50c4a6d6-940b-4c6a-a376-aea2ae2d3168	21,003	c2a461b1-0c15-4047-9fcb-1f966fe55100	97,499	c838aec3-03ef-4398-b882-0e3912abff0	1,265,624
cd2a2e8d-be1c-42e5-b2cd-162caa1c4ce7	255,901	e40c6272-af77-4a10-9385-62a398884f27	65,088	3a29c3df-b45a-403d-bd76-259640245432	4,992
19e46756-9100-4e01-8b0e-23b557558a4c	66,985	ed11cc3e-2947-407c-883c-c53b043917c3	8,573	61d327d1-2227-4c5f-9367-e3559dc79b07	796
70e4f35b-c98c-45a1-9aa9-2053b07315dd	40,815	715327a6-7978-4896-ba91-69d6b04d8bbf	40,191	eeacb0c1-2217-4cf6-b8ce-1f0fedf1b569	9,337
c5ac3ec2-24b0-43cc-9aab-bb0ebbe205ce	4,992	a6046b15-a095-43b0-9fb5-b36899d87fbd	4,992	0fe5eed4-becb-4c00-a388-00bc1455a9b7	4,992
bac09168-940b-4b11-8d55-b4955f80b98d	12,461	f9cfac8d-bfff-47a2-a1f6-503827d375f5	637	43aa19d2-c723-4822-979d-d2f0239835e0	37,121
095940cb-7422-4510-96e2-cbafd961eb88	52,045	30f5e171-83d7-4f0c-bf75-384f122346b3	1,790	3079e9b0-c6db-45c8-b998-a4555a73968e	28,943
79884ae5-e026-4d4a-858f-e80796b0d4f7	4,425	489318a0-24c3-4f5c-b105-f084ed0ea026	13,900	0920bcb8-4b3a-4e9d-a353-56f529fd3b32	48,478
d551b400-b2e5-454d-b5a9-ecce03e6b4739	4,992	a7b4f565-691d-43ea-bf4a-d2d1d52bb4b4	27,111	93091496-be48-4122-b945-9af9e22a7535	28,718
b9b592d4-a0cc-4694-8704-a6625829ef1f	4,992	34229bdc-a895-4394-8820-574e4028d8c6	31,924	01209dce-3575-4bed-b1df-129f5fbc031	51,876
31f657dc-1875-4c4b-a5ca-ce63b3ef3a82	121,916	e5f5d954-cf0e-4bd8-9346-81ddf15a08b	2,487	879bb6df-cc2a-40f1-854b-5be9629d03b2	4,992
edbf04a-f1dd-496a-8237-df11d70621ca	77,525	06ef6b36-6c9b-4e10-8a94-d0baf274276e	10,533	79527108-1f6c-4152-af60-1fcd2e02ba3	4,992
6f0858e0-c590-4740-b022-c152e7608d66	4,992	9ea768a2-87ab-46b6-a73d-c4e915f25af3	40,268	dee75ca4-8348-471e-bbbe-e2143209e3d0	4,992
949ec7fc-ac54-47c9-bb6f-ee9e67688cce	38,937	0bae7ebf-eb54-46a6-be9a-3461ccecf4c	27,675	1df5fa02-4a6e-4b00-a203-cb0a60e75637	4,992
729f397a-0812-4b52-a7d1-b377107ff41	4,992	53d62b10-bae5-48ac-b16e-71be9ba6de59	4,992	364bd0c7-f7fd-48ed-99c1-ae26872b1042	931,012
ae4552dc-e2ea-4d67-b375-03ec7480f780	37,275	fe2479fd-daff-41a8-97dc-a50457ab1871	292,010	50eb1e23-b8d4-4f76-a184-44e5541fa05a	4,775
77c1c785-809f-4065-8c54-6a0170783256	37,767	49108ba9-1b7a-4a8a-9859-3d32e6a83926	4,992	39ed7d98-676d-4b8d-9d0a-0f3b60914ead	118,647
dd03ce70-3243-4c96-9561-330cc461e4d7	23,732	00ba8341-48ec-4e4e-bb56-be0dd2dd7913	4,992	9ddea8d9-cc4c-420a-90f6-880996f808d4	100,307
9dbab10c-118d-496b-966a-67f1763a6b7d	1,462,702	ca421096-6240-4cee-8c12-d20899b3e005	81,736	731e6380-879f-4b0b-9a1f-2150208852ef	2,065
43245158-5ae1-4e71-a9a6-67eeaf9c26bc	113,304	f801b7a9-80a6-4d09-9161-71474deb58ae	6,044	54801477-ac3e-47e3-8170-96c5b40d5c10	4,992
43848156-ba94-47b5-8409-7535cea75678	4,992	c5cfa2b7-abb1-4a50-908f-707b54ca606b	14,094	1cf24082-59de-4029-ac81-6e398768af3a	29,522
978a566a-dc27-478d-b306-26dabal16c1f	1,102,250	726afd49-df7b-4b56-967a-0fb79d85ee4b	4,992	9adb1b29-65a2-4dd0-86bf-c02690d65fbd	4,992
e6361237-ac4e-4c5d-ad8f-f16aca0c0a8f	66,719	344f27ab-428c-4a0e-a7e1-d4441f2f9b80	4,992	af8b241a-c72c-4470-b14a-80e7336c6ab6	4,335
346c5aad-b034-4248-8cbe-0a05fd634b9c	163,779	529bb209-9d7b-44da-bfa4-f6e4745c46c2	32,678	33da10b0-9c1d-4c82-9b14-c67cdf9fae5	30,022
d98ea49e-b70d-4434-b850-bbe217c9b66e	15,216	5e57cd50-8e42-42d6-940d-5c166d006864	693,682	3e55180c-780a-4424-9434-5296640ffcd0	7,774
f3c49918-4707-4d92-bb6d-2b5b4eb9d1b4	15,177	c5cddbbb-8ba4-4338-8b34-15edb5231e22	4,992	b617ee1b-f8c8-4de9-b82b-e803ab93550d	391,963
9f499d32-400d-4c42-ac9a-fb1481844fee	56,367	93131426-0124-4ab4-a013-9dfbc99d467	24,327	abd889c6-f60a-4fbd-924e-ee1e9dcf909b	4,992
2f6a20f1-173d-4b8d-860b-c47f1ea120fa	2,868	75548d10-160d-4f3e-b317-99ad9630c62d	4,992	e84f2780-51e8-4cfa-8aa0-13bbf6f77c7	167,598
be401db3-d732-408a-b0c4-71af0458b8ab	135,462	6e9e3264-02e1-455a-840b-4fbcee132ae7	4,992	639ffc23-14db-4060-9027-3c90314200f8	35,290
4724c395-0c46-46d2-81f7-60fd271fb488	35,350	4fd2ee79-ab3a-4827-a773-1b7cd099307	4,992	c7775e88-49bf-4ba2-a03b-93f00447c958	647,366
15c5e186-df92-4b17-a253-199e10ffe98a	4,992	019c7af2-c827-4454-9970-44d5e39ce068	12,590	8c42cfd0-0b0a-46d5-910c-fc833d38c45e	65,662
1b767f95-d0a0-4a3d-b394-cc665d86c3dc	34,933	b3c55d0d-4529-4b61-b485-29026be0e4e	4,992		
Total: 10,010,835					

Table 4: Distribution of datapoints in evaluation datasets from Tabula Sapiens v2 benchmark (Tabula Sapiens Consortium et al., 2022).

Tissue	Number of Cells	Tissue	Number of Cells
Bladder	36,715	Blood	17,802
Bone Marrow	8,045	Ear	3,055
Eye	21,121	Fat	71,021
Heart	13,344	Large Intestine	15,231
Liver	10,002	Lung	11,716
Lymph Node	72,290	Mammary	18,539
Muscle	13,035	Ovary	48,942
Prostate	2,044	Salivary Gland	11,561
Skin	6,486	Small Intestine	25,834
Spleen	30,690	Stomach	33,064
Testis	7,513	Thymus	9,933
Tongue	21,499	Trachea	5,346
Uterus	10,580	Vasculature	23,569
Total			548,977

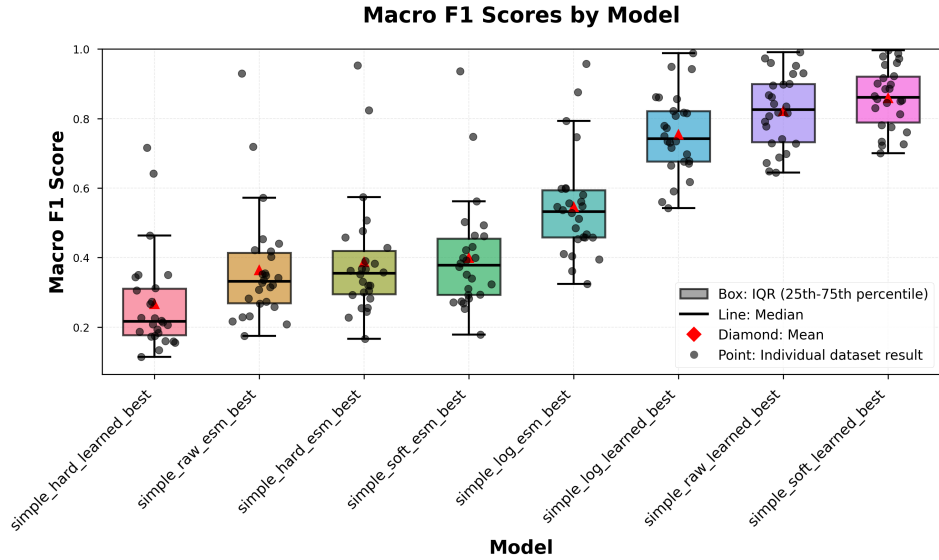


Figure 1: Boxplot of macro F1 score distribution by gene and expression encoding methods. Each point represents a macro F1 score for a kNN classifier trained on one of the evaluation datasets (Table 4) with a fixed trained transformer model.

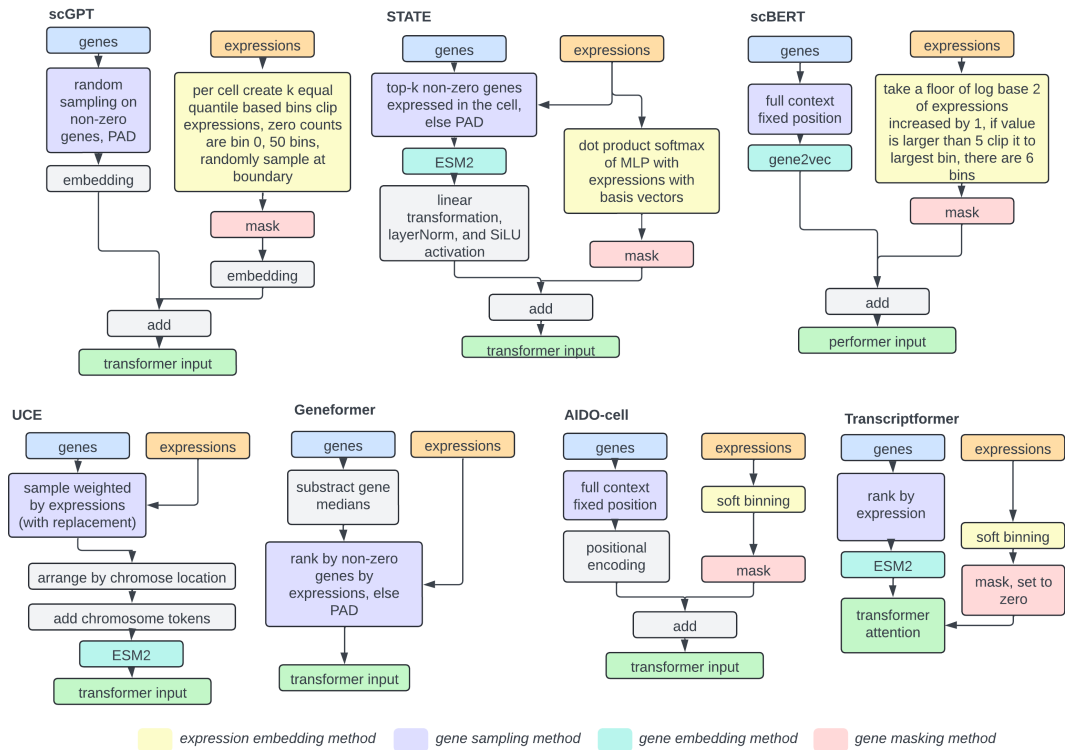


Figure 2: Schematic comparison of different gene and expression encoding methods across single cell foundational models (Cui et al., 2024; Adduri et al., 2025; Ho et al., 2024; Wang et al., 2021; Theodoris et al., 2023; Pearce et al., 2025; Rosen et al., 2023).